Available online at www.sciencedirect.com
ScienceDirect
Journal of Solid State Chemistry 181 (2008) 730–734
JOURNAL OF SOLID STATE CHEMISTRY
www.elsevier.com/locate/jssc

Cation-dependent anomalous compression of gallosilicate zeolites with CGS topology: A high-pressure synchrotron powder diffraction study

Yongjae Lee[a,*], Hyun-Hwi Lee[b], Dong Ryeol Lee[b], Sun Jin Kim[c], Chi-chang Kao[d]

[a]*Department of Earth System Sciences, Yonsei University, Seoul 120-749, Republic of Korea*
[b]*Pohang Accelerator Laboratory, POSTECH, Pohang 790-784, Republic of Korea*
[c]*Nano-Materials Research Center, Korea Institute of Science and Technology, Seoul 136-791, Republic of Korea*
[d]*National Synchrotron Light Source, Brookhaven National Laboratory, Upton, NY 11973, USA*

Received 12 September 2007; received in revised form 29 November 2007; accepted 7 January 2008
Available online 17 January 2008

Abstract

The high-pressure compression behaviour of 3 different cation forms of gallosilicate zeolite with CGS topology has been investigated using in situ synchrotron X-ray powder diffraction and a diamond-anvil cell technique. Under hydrostatic conditions mediated by a nominally penetrating pressure-transmitting medium, unit-cell lengths and volume compression is modulated by different degrees of pressure-induced hydration and accompanying channel distortion. In a Na-exchanged CGS ($Na_{10}Ga_{10}Si_{22}O_{64}\cdot 16H_2O$), the unit-cell volume expands by ca. 0.6% upon applying hydrostatic pressure to 0.2 GPa, whereas, in an as-synthesized K-form ($K_{10}Ga_{10}Si_{22}O_{64}\cdot 5H_2O$), this initial volume expansion is suppressed to ca. 0.1% at 0.16 GPa. In the early stage of hydrostatic compression below ~1 GPa, relative decrease in the ellipticity of the non-planar 10-rings is observed, which is then reverted to a gradual increase in the ellipticity at higher pressures above ~1 GPa, implying a change in the compression mechanism. In a Sr-exchanged sample ($Sr_5Ga_{10}Si_{22}O_{64}\cdot 19H_2O$), on the other hand, no initial volume expansion is observed. Instead, a change in the slope of volume contraction is observed near 1.5 GPa, which leads to a 2-fold increase in the compressibility. This is interpreted as pressure-induced rearrangement of water molecules to facilitate further volume contraction at higher pressures.

Keywords: Gallosilicate zeolites; CGS; Synchrotron X-ray diffraction; High-pressure; Anomalous volume contraction

1. Introduction

The CGS topology belongs to a few classes of microporous materials that are unique to gallosilicate and gallophosphate chemistry [1–3]. Among those, gallosilicate TsG-1 was first reported by Krutskaya et al. [4] while studying the phase diagrams of the K_2O–Ga_2O_3–SiO_2–H_2O system at 200 °C. The openings to the cages in the CGS topology are combinations of non-planar elliptical 8- and 10-rings (Fig. 1), similar to those found in clinoptilolite and suggest that it might exhibit clinoptilolite-like selectivity towards Sr^{2+} and Cs^+ ions. The selectivity of the CGS framework toward Sr cations was then confirmed by competitive ion-exchange experiments performed using a Sr^{2+}:Na^+ = 1:5 solution, in situ ion chromatography and in situ X-ray diffraction [5].

The ion-exchange properties of zeolites are generally controlled by factors such as the anionic field strength of the framework and the free energy of hydration of the exchanging cations [6]. Other factors important in determining the ion-exchange selectivity include structural parameters, such as the framework geometry and connectivity. Temperature has been extensively used to control such factors and thereby to tune ion-exchange properties. Pressure, on the other hand, has been neglected although it can be equally important to modify cation selectivity. Applying pressure affects not only the sizes and shapes of the cages and channels, but also the hydration levels and cation coordination environments, which need to be

*Corresponding author. Fax: +82 2 392 6527.
E-mail address: yongjaelee@yonsei.ac.kr (Y. Lee).

0022-4596/$ - see front matter © 2008 Elsevier Inc. All rights reserved.
doi:10.1016/j.jssc.2008.01.017

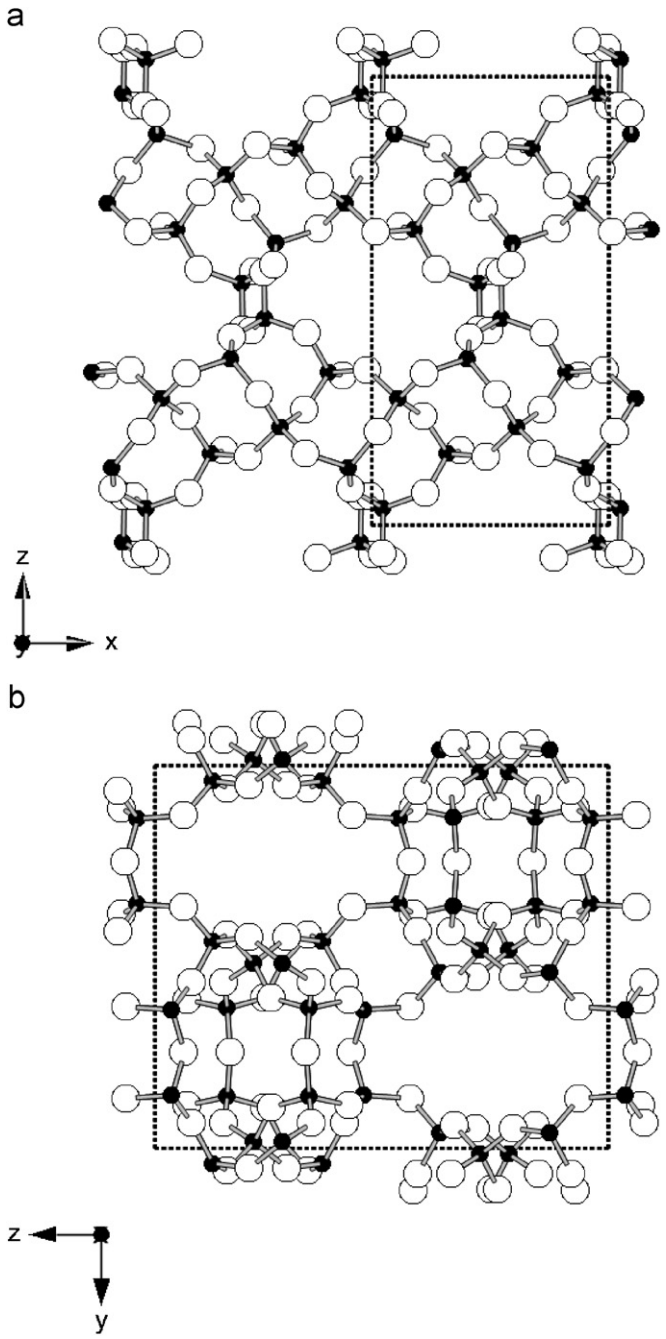

Fig. 1. Ball-and-stick representations of the gallosilicate CGS viewed (a) along the *b*-axis and (b) along the *a*-axis. Filled circles represent Ga/Si tetrahedral atoms and open circles oxygen atoms. Cations and water molecules are omitted for clarity. The structure model is from the single crystal study on K-CGS by Lee et al.

negotiated during the ion-exchange process. Recent studies show that even minor changes in water vapour pressure near ambient conditions can cause different levels of hydration and structural phase transitions in zeolites [7,8].

As a first step toward understanding of the ion-exchange properties under pressure, we have performed comparative high-pressure compression experiments on 3 different cation forms of gallosilicate CGS up to 5 GPa using in situ synchrotron X-ray powder diffraction and diamond-anvil cell technique. In order to allow the variation of water content under pressure, nominally pore-penetrating hydrostatic pressure medium of alcohol and water mixture was used. We report here anomalous volume contraction behaviour of gallosilicate CGS that is apparently affected by the cation type and its initial hydration level.

2. Experimental methods

2.1. Materials

Potassium gallosilicate CGS (K-CGS) was synthesized in a manner similar to that described by Lee et al. [3]. To prepare strontium form of gallosilicate CGS (Sr-CGS), ion exchange was performed using 0.1 g of as-synthesized single crystals (150 μm maximum dimension) of K-CGS and 500 ml of 0.1 M $SrCl_2 \cdot 6H_2O$ solution adjusted to pH 9 with $Sr(OH)_2 \cdot 8H_2O$. The solution passed at 0.1 ml/min through a 1.0 mm diameter glass capillary, where the single crystals were held in place in-between glass fibres at both ends. This procedure was chosen to maximize the amount of the solution contacting the crystals without stirring [5]. Three days of ion exchange at room temperature completely removed all residual potassium cations from the crystals, as determined from electron probe micro-analysis (EPMA). Sodium form of gallosilicate CGS (Na-CGS) was prepared using 0.5 M NaCl solution in a similar manner as described above. The water contents of K-CGS, Na-CGS, and Sr-CGS were determined via single crystal diffraction data, TG analysis, and powder Rietveld refinement, respectively [3,5]. This gives rise to ideal unit-cell formula of $K_{10}Ga_{10}Si_{22}O_{64} \cdot 5H_2O$, $Na_{10}Ga_{10}Si_{22}O_{64} \cdot 16H_2O$, and $Sr_5Ga_{10}Si_{22}O_{64} \cdot 19H_2O$ for K-CGS, Na-CGS and Sr-CGS, respectively. Each CGS sample was then grinded and equilibrated over the vapour pressure of a saturated NH_4NO_3 solution for a week prior to the high-pressure synchrotron X-ray powder diffraction experiment. Powder XRD patterns of the 3 CGS samples measured at ambient conditions are compared in Fig. 2.

2.2. High-pressure synchrotron X-ray powder diffraction

In situ high-pressure synchrotron X-ray powder diffraction experiments on K-CGS and Sr-CGS were performed at the X7A beamline at the National Synchrotron Light Source (NSLS) at Brookhaven National Laboratory (BNL). The primary white beam from the bending magnet was focused in the horizontal plane by a triangular Si (111) monochromator bent to a cylindrical curvature by applying a load to the crystal tip, creating ~200 μm focused monochromatic radiation of 0.6474 Å. A tungsten wire crosshair was positioned at the centre of the goniometer circle and subsequently the position of the incident beam was adjusted to the crosshair. A gas-proportional position-sensitive detector covering 4° in 2θ was stepped in 0.25° intervals over the angular range of 3.5–33.5° with counting

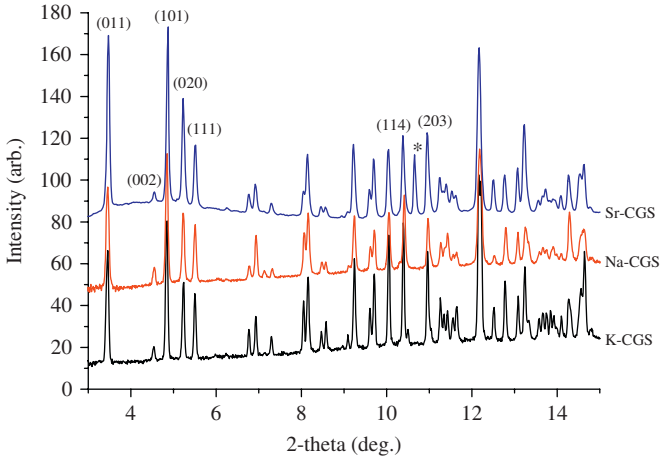

Fig. 2. Powder diffraction patterns of K-CGS, Na-CGS and Sr-CGS measured at ambient pressure at room temperature.

times of 90–150 s per step. The wavelength of the incident beam was determined from a CeO_2 standard (SRM 674).

A modified Merrill–Bassett diamond-anvil cell (DAC) was used for the high-pressure experiments, equipped with 2 type-I diamonds anvils (culet diameter of 500 μm) and tungsten-carbide supports. Stainless-steel foil of 250 μm thickness was pre-indented to a thickness of about 100 μm, and a 200 μm diameter hole was obtained by electro-spark erosion. Each powdered sample of K-CGS and Sr-CGS were placed in the gasket hole together with some ruby chips for the pressure measurements. The pressure at the sample was measured by detecting the shift in the R1 fluorescence line of the included ruby chips (precision: ±0.05 GPa). A methanol:ethanol:water (16:3:1 by volume) mixture was used as hydrostatic pressure-transmitting medium. The sample was equilibrated for about 10 min at each measured pressure, and after the diffraction data measurement, the pressure was raised by ~0.5 GPa increments.

High-pressure diamond-anvil cell experiment on Na-CGS was performed at the multi-purpose wiggler beamline 5 A at Pohang Accelerator Laboratory. A monochromatic synchrotron beam of 0.6888 Å in wavelength and 200 μm in diameter was provided by a sagitally focusing monochromator and mirrors. Each diffraction data was measured for 1 min on MAR345 imaging plate, and the data were processed using the Fit2d suite of programs [9].

The pressure-induced variations of unit-cell constants and volume were analysed by full profile fitting methods using the GSAS suite of programs [10,11]. The background was modelled with linear interpolation between fixed points. The pseudo-Voigt profile function proposed by Thompson et al. [12] was used to fit the experimental peak shape. Rietveld analysis using high-pressure data were not successful due to low counting statistics and poor powder averaging effects. No evidence of pressure-induced amorphization was detected from the evolution of the powder patterns measured up to 5 GPa.

3. Results and discussion

The evolutions of the unit-cell constants of 3 cation forms of gallosilicate CGS with pressure are shown in Fig. 3. The orthorhombic lattice is maintained within the pressure-range investigated. In all cases, the changes in the *a*-axis length are characterized by normal linear compression with pressure. This is the direction where the periodic 4-ring building units are arranged in a dense one-dimensional chain (Fig. 1) and cations form arrays occupying the buckled 8-ring sites. On the other hand, the *b*-axis length exhibits anomalous changes with pressure and this seems to vary with the cation type. In Na-CGS, the *b*-axis initially expands by ca. 0.4% upon applying hydrostatic pressure. In K-CGS, the initial expansion in the *b*-axis length is marginal, and further increase in pressure leads to a progressive contraction in the *b*-axis length. In Sr-CGS, no clear expansion or contraction in the *b*-axis length is observed up to ca. 1.5 GPa, where the *b*-axis length starts to decrease. Interestingly, the *c*-axis length appears to exhibit the opposite behaviour to that of the *b*-axis length. Especially in K-CGS, the initial increase and subsequent 'slow' decrease in the *b*-axis length below 1 GPa is coupled with a rather 'fast' decrease in the *c*-axis length. This seems to be related to the compression mechanism of the non-planar elliptical 10-rings in the *bc*-plane of the CGS framework. The 'relative increase' in the *b*-axis, which is introduced by a 'slow' decrease in the *b*-axis length and a 'fast' decrease in the *c*-axis length below 1 GPa, would result in the decrease in the ellipticity of the non-planar 10-rings. During this period, the 10-ring channel along the *a*-axis would become more circular and facilitate additional hydration by the uptake of water molecules from the hydrostatic pressure medium. Above 1 GPa, the anisotropic compression behaviour of the *bc*-plane is reversed and a 'fast' decrease in the *b*-axis length and a 'slow' decrease in the *c*-axis length increases the ellipticity of the non-planar 10-rings. In this stage, pressure-induced hydration would have been completed and further compression leads to the distortion of the 10-ring channels. The reason why there is no immediate expansion in the *b*-axis length in Sr-CGS might be related to its higher initial water content at ambient conditions (19 H_2O per unit cell) compared to those of K-CGS and Na-CGS. In Sr-CGS, the initial decrease in the ellipticity of the non-planar 10-rings, as manifested by the decrease in the *c*-axis length with marginal decrease in the *b*-axis length below 1.5 GPa, might exert rearrangement of the fully-occupied water molecules. Above 1.5 GPa, the ellipticity of the 10-ring channels reverts to increase, as observed in K-CGS, and this becomes the dominant compression mechanism.

Volume compressibility was calculated using the Birch–Murnaghan equation of state (BM-EoS) [13], which is based upon the assumption that the high-pressure strain of a solid can be expressed as a Taylor series in the Eulerian strain,

$$f = [(V_0/V)^{2/3} - 1]/2,$$

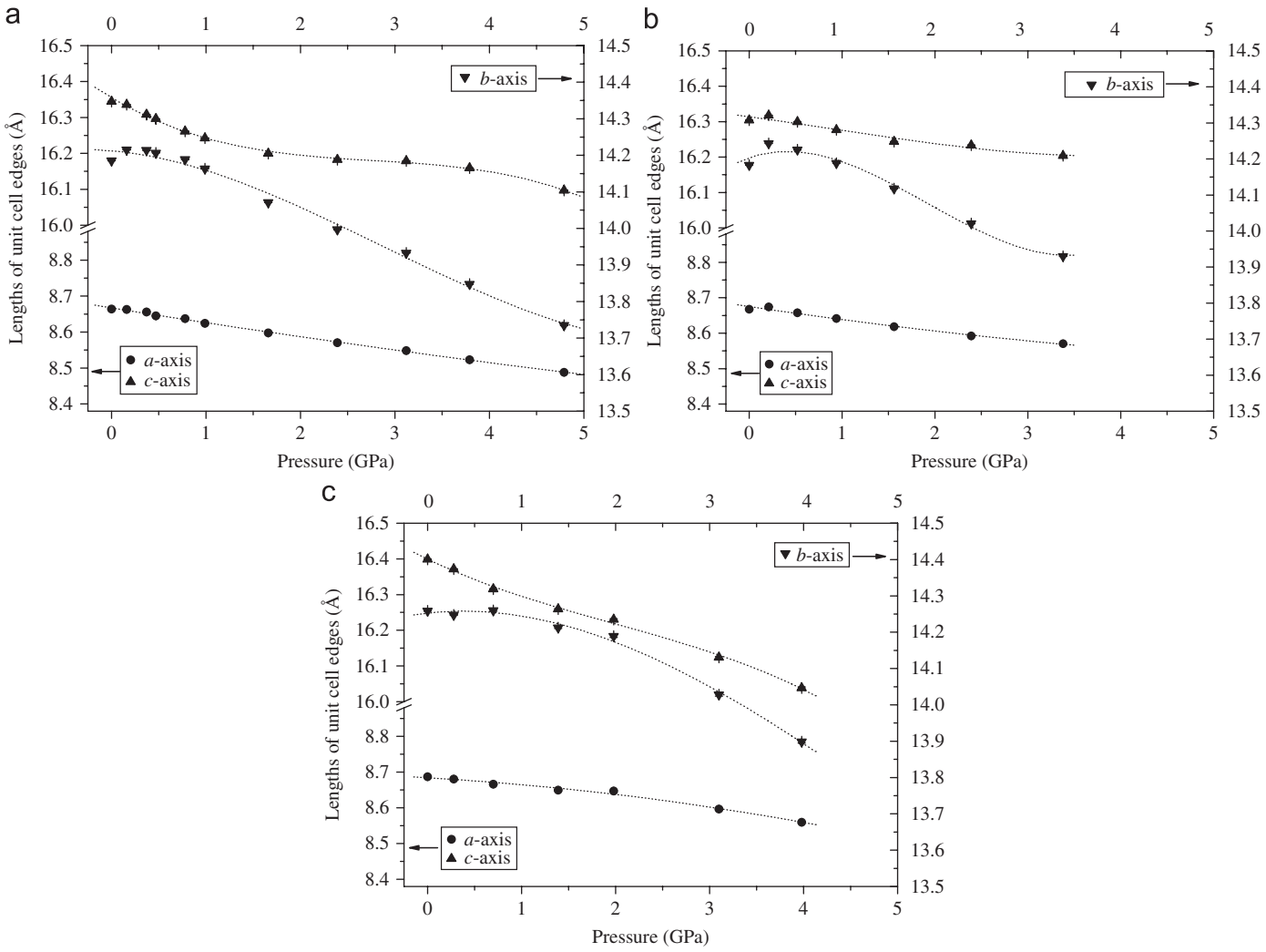

Fig. 3. Pressure-induced changes in the unit-cell edge lengths in (a) K-CGS, (b) Na-CGS, and (c) Sr-CGS. Dotted lines are guides to the eyes. Estimated standard deviations are smaller than the symbols and are omitted for clarity.

where V_0 and V represent the unit-cell volume, under ambient and high-pressure conditions, respectively. Expansion in the Eulerian strain yields the following isothermal EoS:

$$P(f) = 3K_0 f(1+2f)^{5/2}\{1 + 3/2(K' - 4)f + 3/2 [K_0K'' + (K' - 4)(K' - 3) + 35/9]f^2 + \cdots\},$$

where K_0 represent the bulk modulus, defined as $K_0 = -V_0(\partial P/\partial V)_{P=0} = 1/\beta$, where β is the volume compressibility coefficient, and K' and K'' represent its pressure derivatives ($K' = \partial K_0/\partial P; K'' = \partial^2 K_0/\partial P^2$). Due to the low-pressure-range investigated and small volume reduction at the maximum pressure (less than 7%), the P–V data of gallosilicate CGS were fitted with a truncated second-order BM-EoS with K' fixed at 4 (Fig. 4). In addition, in order to account for the apparently increased hydration level at the starting pressures, $V_{0.16}$ and $V_{0.21}$ were taken as V_0 in K-CGS and Na-CGS, respectively, and hence the derived

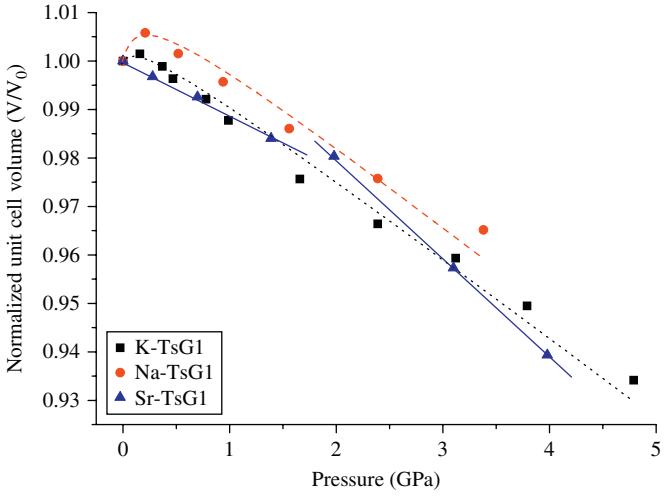

Fig. 4. BM-EoS fits to the normalized unit-cell volumes in K-CGS (squares + dotted line), Na-CGS (circles + dashed lines), and Sr-CGS (upper triangles + straight lines). Each line is a guide to the eyes.

Table 1
Changes in the unit cell lengths of K-CGS, Na-CGS and Sr-CGS as a function of applied hydrostatic pressure mediated by alcohol and water mixture at room temperature

	a (Å)	b (Å)	c (Å)	V (Å^3)
K-CGS (GPa)[a]				
0	8.6638(2)	14.1853(4)	16.3444(4)	2008.7(1)
0.47	8.6449(2)	14.2068(4)	16.2960(4)	2001.4(1)
0.99	8.6246(2)	14.1634(4)	16.2424(4)	1984.1(1)
1.66	8.5977(2)	14.0711(4)	16.2000(4)	1959.8(1)
2.39	8.5705(2)	13.9970(4)	16.1824(5)	1941.3(1)
3.12	8.5487(3)	13.9328(5)	16.1787(6)	1927.0(2)
3.79	8.5232(3)	13.8478(6)	16.1593(7)	1907.2(2)
4.79	8.4877(6)	13.735(1)	16.097(1)	1876.5(4)
Na-CGS (GPa)[a]				
0	8.6677(3)	14.1833(5)	16.3038(6)	2004.3(2)
0.21	8.6743(3)	14.2432(6)	16.3175(6)	2016.0(2)
0.52	8.6577(4)	14.2255(6)	16.2991(7)	2007.4(2)
0.94	8.6415(5)	14.1886(8)	16.2770(9)	1995.7(3)
1.56	8.6184(4)	14.1181(7)	16.2434(8)	1976.4(2)
2.39	8.5925(6)	14.0210(9)	16.2335(9)	1955.7(3)
3.38	8.5705(4)	13.9301(6)	16.2038(6)	1934.5(2)
Sr-CGS (GPa)[a]				
0	8.6872(6)	14.2585(9)	16.399(1)	2031.3(3)
0.28	8.6803(8)	14.248(1)	16.371(1)	2024.7(4)
0.70	8.666(1)	14.260(2)	16.315(1)	2016.2(6)
1.39	8.650(2)	14.213(3)	16.259(2)	1998.8(7)
1.98	8.647(2)	14.189(3)	16.230(2)	1991(1)
3.10	8.597(2)	14.028(4)	16.124(3)	1945(1)
3.98	8.560(2)	13.899(4)	16.038(3)	1908(1)

[a]Space group *Pnma* was used throughout.

bulk moduli would represent those of the volume-expanded phases (Table 1 and Fig. 4). In the case of Sr-CGS, however, a clear change in the slope of the V/V_0 plot is seen near 1.5 GPa, as discussed above in the pressure-induced evolution of the unit-cell constants, and the bulk modulus was fitted separately for the low- and high-pressure region (Fig. 4).

The derived bulk modulus of K-CGS, 59(1) GPa, is comparable to 69(1) GPa of Na-CGS. This implies that the geometry of the hydration shell after pressure-induced hydration would become more or less similar and experience similar distortions under pressure with respect to the host framework. The bulk moduli of Sr-CGS are fitted to 85(2) and 43(1) GPa for the low- and high-pressure region, respectively. We argue here that, near 1.5 GPa, the compression mechanism changes from water rearrangement to framework distortion and partial collapse of the 10-ring channel, resulting in the observed doubling in the compressibility. High-pressure structural studies would clarify the proposed high-pressure chemistry as well as the accompanying changes in the compression mechanism.

4. Conclusion

When mediated by pore-penetrating pressure medium, gallosilicate CGS shows different compression behaviour depending on the cation type as well as the initial hydration level. Pressure-induced hydration and volume expansion occur in the early stage of hydrostatic compression in the potassium and sodium forms of CGS via decreasing the ellipticity of the 10-ring channels. The ellipticity then reverts to increase at further compression above 1 GPa, thereby limiting the access to the 10-ring channels. The initial higher water content in the strontium-exchanged CGS results in no apparent volume expansion under hydrostatic compression. Furthermore, the observed increase in the compressibility above 1.5 GPa implies a change in the compression mechanism, possibly related to the rearrangement of the water molecules. These anomalous compression behaviours point toward subsequent modifications in the cation selectivity and need to be considered in the high-pressure ion exchange.

Acknowledgments

This work was supported by the Korea Research Foundation Grant funded by the Korean Government (MOEHRD) (KRF-2006-D00538). Experiments at PAL were supported in part by Ministry of Science and Technology (MOST) of the Korean Government and Pohang University of Science and Technology (POSTECH). Research carried out in part at the NSLS at BNL is supported by the US Department of Energy, Office of Basic Energy Sciences.

References

[1] A.M. Chippindale, A.R. Cowley, Microporous Mesoporous Mater. 21 (1998) 271.
[2] S.B. Hong, S.H. Kim, Y.G. Kim, Y.C. Kim, P.A. Barrett, M.A. Camblor, J. Mater. Chem. 9 (1999) 2287.
[3] Y. Lee, S.J. Kim, G. Wu, J.B. Parise, Chem. Mater. 11 (1999) 879.
[4] T.M. Krutskaya, V.E. Morozkova, A.N. Kolishev, Izv. Sib. Otd. An. Khim. 5 (1984) 61.
[5] Y. Lee, S.J. Kim, M.A.A. Schoonen, J.B. Parise, Chem. Mater. 12 (2000) 1597.
[6] R.M. Barrer, Hydrothermal Chemistry of Zeolites, Academic Press, London, 1982.
[7] Y. Lee, S.J. Kim, I. Bull, A.J. Celestian, J.B. Parise, C.-C. Kao, T. Vogt, J. Am. Chem. Soc. 129 (2007) 13744.
[8] Y.V. Seryotkin, V.V. Bakakin, Eur. J. Mineral. 19 (2007) 593.
[9] A.P. Hammersley, FIT2D: V9.129 Reference Manual V3.1, 1998.
[10] A.C. Larson, R.B. VonDreele, General structure analysis system (GSAS), Report LAUR 86-748, Los Alamos National Laboratory, New Mexico, 1986.
[11] B.H. Toby, J. Appl. Crystallogr. 34 (2001) 210.
[12] P. Thompson, D.E. Cox, J.B. Hastings, J. Appl. Crystallogr. 20 (1987) 79.
[13] F. Birch, J. Geophys. Res. 83 (1978) 1257.